Agricultural Water Management 259 (2022) 107242

Contents lists available at ScienceDirect

Agricultural Water Management

journal homepage: www.elsevier.com/locate/agwat

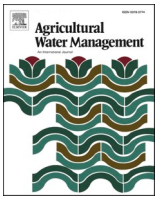

Seasonal variation and controlling factors of evapotranspiration over dry semi-humid cropland in Guanzhong Plain, China

Yunfei Wang [a,b,c,1], Yufeng Zou [a,1], Huanjie Cai [a,*], Yijian Zeng [c], Jianqiang He [a], Lianyu Yu [c], Chao Zhang [d], Qaisar Saddique [a], Xiongbiao Peng [a], Kadambot H.M. Siddique [e], Qiang Yu [b], Zhongbo Su [c]

[a] College of Water Resources and Architectural Engineering, Northwest Agriculture and Forestry University, Yangling, China
[b] State Key Laboratory of Soil Erosion and Dryland Farming on the Loess Plateau, Institute of Water and Soil Conservation, Northwest Agriculture and Forestry University, Yangling, China
[c] Faculty of Geo-Information Science and Earth Observation, University of Twente, Enschede, The Netherlands
[d] College of Hydraulic, Energy and Power Engineering, Yangzhou University, Yangzhou 225009, China
[e] The UWA Institute of Agriculture, The University of Western Australia, Perth, WA 6001, Australia

ARTICLE INFO

Handling editor - Dr. B.E. Clothier

Keywords:
Evapotranspiration
Eddy covariance
Canopy conductance
Controlling factors
Guanzhong plain

ABSTRACT

The Guanzhong Plain is a critical food production area in the Yellow River Basin that frequently suffers from water shortages. In this study, long-term (June 2013 to June 2018) water and energy fluxes were observed, and path analysis was conducted over an irrigated winter wheat (*Triticum aestivum* L.) / summer maize (*Zea mays* L.) rotation field to identify the controlling factors of evapotranspiration (ET). Total ET for each crop year ranged from 627 to 775 mm, with an average growing season ET of 398 mm for wheat and 310 mm for maize. There is significant seasonal variation in both ET and surface conductance (G_s). Daily ET varied from 0.0 to 6.0 mm d^{-1} for wheat and 0.0 to 6.7 mm d^{-1} for maize. The peak daily values of G_s were 29.5 mm s^{-1} for wheat and 19.5 mm s^{-1} for maize. The direct and indirect effects of environmental and biological factors—net radiation (R_n), surface conductance (G_s), saturation vapor pressure deficit (VPD), leaf area index (LAI), air temperature (T_{air}), and volumetric soil water content (VWC)—on ET were calculated using the path analysis method. R_n was determined to be the primary controlling factor of ET for both the summer maize and winter wheat growing seasons. Also, G_s was found to be another controlling factor that has more controlling power in the summer maize growing season than in the winter wheat season. VPD had a significant positive and direct effect on ET for both of the crop seasons, while it had a significant negative and indirect effect on ET through G_s in the summer maize season. VWC and T_{air} only directly affected the wheat ET. In addition, VWC had two significant paths that can indirectly affect ET through LAI and G_s. The revealed seasonal patterns and controlling factors of evapotranspiration in this agroecosystem provide a theoretical basis for optimizing water resources management of the Yellow River.

1. Introduction

Evapotranspiration (ET) plays a vital role in the hydrological cycle and energy partitioning in agricultural ecosystems. Identifying and understanding seasonal variation in water flux and energy partitioning is essential to determine controlling factors of water and energy fluxes at different spatial and temporal scales (Burba and Verma, 2005). Where water resources are scarce, an in-depth study of ecohydrological processes (especially ET) is of paramount importance for efficient water use. A large amount of cropland irrigation can change the regional energy balance and water cycles, which affect the regional microclimate (Prueger et al., 1996). Therefore, studying the variation in water and energy fluxes, which are influenced by human activities (e.g., irrigation), is helpful to understand the regional water cycle (Lei and Yang, 2010).

The eco-hydrological processes underlying the soil–plant–atmosphere continuum are controlled by meteorological factors (e.g., net radiation, vapor pressure deficit, air temperature), hydrological factors

* Correspondence to: College of Water Resources and Architectural Engineering, Northwest A&F University, Yangling, Shaanxi 712100, China.
E-mail address: caihj@nwsuaf.edu.cn (H. Cai).
[1] Yunfei Wang and Yufeng Zou contributed equally to this work.

https://doi.org/10.1016/j.agwat.2021.107242
Received 26 May 2021; Received in revised form 3 October 2021; Accepted 4 October 2021
Available online 13 October 2021

(soil water content), and biological factors (leaf area index and stomatal conductance) (Zha et al., 2013). While it was upscaled to the canopy, water and carbon exchanges are determined by the relationship between surface conductance (G_s) and aforementioned factors (Marques et al., 2020). For given available radiation, the surface vapor conductance or G_s is the key parameter that controlling the magnitude of evapotranspiration in most land surface models (Salvucci and Gentine, 2013). Better understanding of G_s not only reveals the mechanisms underlying water and carbon exchange of land surface, but also is helpful for future applications of ET models under the conditions in which G_s need to be calculated (Marques et al., 2020). Quantifying G_s and studying its relationship with ET remain challenging because it is influenced by climate pattern and vegetation species (Tan et al., 2019). Therefore, it is essential to study the differences of mechanisms of G_s response to meteorological, biological, and hydrological factors among different vegetation types. In addition, previous studies only studied the relationship between G_s and aforementioned factors but ignored the inner relationship among these factors (Lei and Yang, 2010; Ma et al., 2015; Ryu et al., 2008; Suyker and Verma, 2008; Tan et al., 2019; Zha et al., 2013). Recently, some studies have focused on revealing the main controlling factors considering the inner relevance of the ecohydrological factors, although such studies are challenging (Tian et al., 2016; Massmann et al., 2019; Marques et al., 2020).

Vapor pressure deficit (VPD) is projected to increase over continents at the end of this century because of the combination of increased temperature and, depending on region, decreased relative humidity (Byrne and O'Gorman, 2013). High VPD increases the atmospheric demanding of ET (Monteith, 1965; Penman, 1948) as well as reduces stomatal aperture (Damour et al., 2010). Therefore, there are two possible perspectives for how ET responds to VPD (Massmann et al., 2019). On the one hand, it is well known that, from a hydrometeorological perspective, higher VPD increases the vapor pressure gradient between land surface and atmosphere, and this leads to an increase ET (Penman, 1948). On the other hand, from a plant physiology perspective, plants' stomata have evolved to optimally regulate the exchange of water and carbon and tend to partially close in response to increased atmospheric dryness (Medlyn et al., 2017), which leads to a decrease in ET (Rigden and Salvucci, 2017). In a word, the question "How does ET respond to VPD?" can be related to whether plant regulation or atmospheric demand dominates the ET response (Massmann et al., 2019).

As an important component of the Yellow River Basin, the Guanzhong Plain, located in Shaanxi Province of Northwest China, is an important food production area that accounts for approximately two-thirds of the entire province's total crop yield (Zhao et al., 2018). The major agricultural system in this region is double-cropping winter wheat/summer maize (Li et al., 2016). The eddy covariance (EC) technique is widely used to directly quantify water flux or ET between the biosphere and atmosphere without destroying the ecosystem (Baldocchi, 2014). This technique is considered dependable for measuring fluxes with high time resolution and accuracy (Baldocchi, 2003). With this technique, we can improve our understanding of ecological and hydrological problems (Baldocchi, 2008, 2014; Korner, 2003; Wofsy et al., 1993). Although many studies have used the EC method to characterize energy and mass fluxes across diverse ecosystems (Baldocchi et al., 2001), none has characterized annual variation and controlling factors of water vapor flux in typical irrigated rotation cropland (winter wheat/summer maize) on the Guanzhong Plain. This area has a dry semi-humid climate. There was high VPD despite the crop being well-watered. Therefore, understanding the ET response to these two opposing effects of VPD (Massmann et al., 2019), especially for this irrigated area, will be useful for quantifying water use and optimizing water source management.

With the EC technique, we conducted energy flux measurements, undertaken on Guanzhong Plain cropland from June 2013 to June 2018, to (1) assess seasonal variability in energy fluxes and determine the energy budget, (2) characterize seasonal and interannual variation in ET, and (3) investigate seasonal and interannual variability in ET and G_s and identify the main controlling environmental and biological factors of ET.

2. Materials and methods

2.1. Study area

The experiment was conducted in an experimental field in Yangling (34°17′ N, 108°04′ E, 521 m a.s.l.) from June 2013 to June 2018 (Fig. 1). The field was approximately 200 m (north to south) by 250 m (east to west). The soil in the study area is a silty clay loam (based on the USDA Soil Taxonomy System) (Zheng et al., 2021) with a field capacity of 0.235 m^3 m^{-3} and bulk density of 1.35 g cm^{-3} (Yu et al., 2016). The groundwater table depth is > 55 m below the soil surface; thus, the water supplied by groundwater was assumed to equal zero. The mean annual temperature at the site is 12.9 °C, and mean annual precipitation is 630 mm (Yu et al., 2016, 2018). The mean annual precipitation during the study period was 599 mm, with 2016 and 2017 being wetter years, 2013 and 2015 being drier years, and 2014 being a relatively normal precipitation year (Table 1). The maximum crop height was approximately 190 cm for summer maize and 90 cm for winter wheat. Summer maize (cv. Wuke No. 2) was planted around 20 June and harvested around 10 October each year, and winter wheat (cv. Xinong 979) was planted around 20 October and harvested around 10 June. Field management operations (i.e., fertilizer application, weed control, and irrigation) followed the local standard management schedule. Nitrogen (typically 180 kg N ha^{-1}) was applied as urea ammonium nitrate solution prior to planting each crop. Flood irrigation was implemented when the crop was under slight water stress (soil moisture less than 70% field capacity). To avoid large amounts of deep percolation, the amount of irrigation was determined by water use (ET minus precipitation) since the last irrigation (Wang et al., 2020a).

2.2. Fluxes and meteorological measurements

The EC system was installed on a height-adjustable tripod. The sensors were positioned 2 m above the soil surface during the wheat growing season and 3 m above the soil surface during the maize growing season (Wang et al., 2020a). The EC system included a three-dimensional sonic anemometer (CSAT-3, Campbell Scientific, Logan, UT, USA) pointed toward the direction of the prevailing wind (providing approximately 120 m of fetch), an open path infrared gas analyzer (LI-7500A, LI-COR, Lincoln, NE, USA), and a datalogger (LI7550, 10 Hz, LI-COR, Lincoln, NE, USA). The system measured both latent and sensible heat fluxes between the ecosystem and atmosphere. Solar radiation was measured by pyranometer. Upward and downward short-wave and long-wave radiation were measured by pyrgeometer, both of which were installed 1.5 m above the soil surface during the wheat growing season and 2.5 m above the soil surface during the maize growing season. Boundary layer meteorological measurements included wind speed and wind direction measured with propeller anemometers (R.M. Young model 03002-5, available from Campbell Scientific, Logan, UT, USA) and air temperature and relative humidity measured with a humidity and temperature probe (model HMP60, Vaisala, Vantaa, Finland) placed 1.5 m and 2.5 m above the soil surface in the wheat and maize growing seasons, respectively. All signals were logged with a CR1000 datalogger (Campbell Scientific) and recorded at 30-min intervals. Soil temperature and soil volumetric water content observations were taken at three depths (20, 40, and 60 cm below the soil surface) using a model 5TM dielectric permittivity meter (METER Environment, Pullman, WA, USA). Rainfall was measured with a tipping bucket rain gauge (model TE525MM-L, Campbell Scientific), snowfall was measured with a weighing type precipitation gauge (model OTT Pluvio, Dusseldorf, Germany), and soil heat flux (G) was measured with a self-tuning heat flux plate (model HFP01SC-L50, Hukseflux, Delft, The

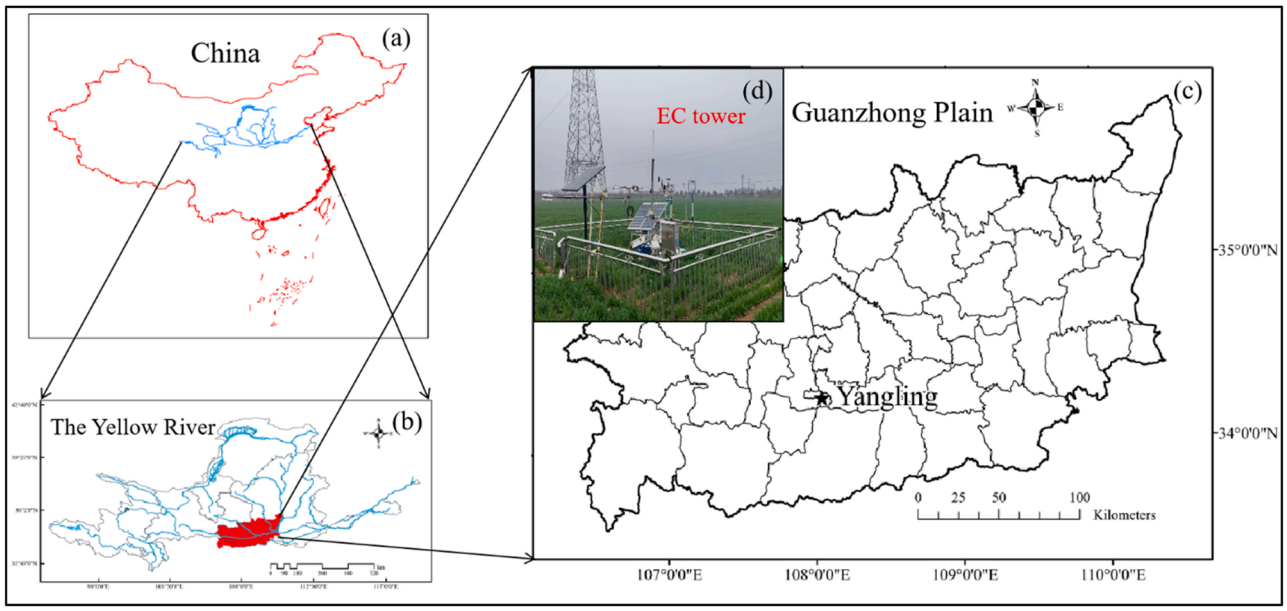

Fig. 1. Location of the research site in Yangling, China. Inset shows the eddy covariance flux tower. (a) The map of China. (b) The map of the Yellow River basin. (c) High-resolution map of the Guanzhong Plain. (d) Picture of the cropland and the Eddy Covariance (EC) tower.

Table 1
Energy fluxes and meteorological conditions during the 5-year study (June 2013 to June 2018) in Yangling, China.

Variable	Year	ET_a (mm)	R_n (MJ m^{-2})	LE (MJ m^{-2})	T_{air} (°C)	VPD (kPa)	β	α	ET_{eq} (mm)	P + I (mm)	VWC (m^3 m^{-3})	LAI_{max} (m^2 m^{-2})
Summer maize	2013	284	1142	693	24.4	1.00	0.55	0.91	311	210 + 93	27.51	5.29
	2014	259	1161	632	23.5	0.99	0.74	0.82	317	394	24.91	5.31
	2015	316	1295	771	22.9	0.91	0.60	0.91	347	284 + 97	25.84	3.59
	2016	372	1353	907	24.8	1.09	0.43	1.00	373	320 + 89	24.01	4.80
	2017	320	1331	779	23.9	1.09	0.60	0.84	379	346 + 91	25.42	4.24
	Average	310	1256	756	23.9	1.02	0.59	0.90	345	311 + 74	28.02	4.96
Winter wheat	2013–2014[a]	361	1344	891	8.9	0.48	0.45	1.23	295	303	22.24	4.59
	2014–2015[a]	368	1601	909	9.3	0.49	0.68	1.20	308	239	22.57	4.93
	2015–2016[a]	437	1593	1080	9.1	0.49	0.42	1.37	320	203 + 95	25.31	4.08
	2016–2017[a]	404	1429	998	9.3	0.47	0.39	1.17	347	385 + 97	25.39	4.12
	2017–2018[a]	420	1652	1037	9.2	0.52	0.54	1.23	342	241 + 90	25.56	4.04
	Average	398	1524	983	9.2	0.49	0.50	1.24	322	274 + 56	25.56	4.35
Annual	2013–2014[b]	645	2486	1584	14.1	0.65	0.50	1.06	606	514 + 93	24.00	5.29
	2014–2015[b]	627	2763	1541	14.0	0.66	0.70	1.00	625	634	23.35	5.31
	2015–2016[b]	753	2888	1851	13.7	0.63	0.50	1.13	667	486 + 192	25.48	4.08
	2016–2017[b]	775	2782	1904	14.5	0.68	0.41	1.08	720	705 + 186	24.93	4.80
	2017–2018[b]	739	2983	1816	14.1	0.71	0.57	1.02	722	586 + 181	25.51	4.24
	Average	708	2780	1739	14.1	0.66	0.53	1.06	668	585 + 130	26.38	4.74

ETa is actual evapotranspiration, Rn is net radiation, LE is latent heat flux, TAIR is air temperature, VPD is air vapor pressure deficit, β is the average daily Bowen ratio, α is the daytime Priestley–Taylor coefficient, ETEQ is equilibrium evaporation, P is precipitation, I is irrigation, VWC is volumetric water content, and Laimax is maximum leaf area index in each growing season.
2013 indicates 10 June 2013–10 October 2013, and so forth for the other four years.
2013–2014[a] indicates 10 October 2013–10 June 2014, and so forth for the other four years.
2013–2014[b] indicates 10 June 2013–10 June 2014, and so forth for the other four years.

Netherlands) located 8 cm below the soil surface. All sensors were calibrated and validated before installation (Wang et al., 2020a, 2020b). The theoretical basis of this EC system can be found in the book published by Aubinet et al. (2012).

Using an LAI-SUNSCAN instrument, we measured leaf area index (LAI) in the wheat and maize growing seasons every two weeks. Owing to the relatively low time-resolution for field observations of LAI, the values were obtained from the NOAA Climate Data Record, derived from a NOAA AVHRR Surface Reflectance product and gridded at a daily resolution of 0.05° https://developers.google.com/earth-engine/datasets/catalog/NOAA_CDR_AVHRR_LAI_FAPAR_V4. The field observations of LAI were used to filter the remotely sensed LAI for outliers, with data gaps filled by linear interpolation.

2.3. Flux data processing

EddyPro software (https://www.licor.com/env/products/eddy_covariance/software.html) was used to process data into 30-min interval turbulent latent (LE) and sensible (H) heat fluxes. Post-processing of EC data included (1) spike detection, (2) time lag correction of H_2O/CO_2, (3) frequency response correction, and (4) coordinate rotation using the planar fit method (Wilczak et al., 2001). During the calculation of flux data, density correction was based on the method presented by Webb et al. (1980). The processed 30-min flux data and meteorological data were screened for anomalous or spurious values caused by system malfunction, power failure, and bad atmospheric conditions, and excluded (Zhang et al., 2016). Based on the quality analysis by EddyPro

software, approximately 23.1% of the flux data recorded from 2013 to 2018 were deleted. Data gaps shorter than 2 h were filled by linear interpolation, and data gaps longer than 2 h were filled using the average daily variation method (Falge et al., 2001). The gap-filling method used in this study could introduce uncertainties to the data, especially during periods of crop rotation. However, as the low-quality data usually occurred in the evening, the systematic bias of filled data has limited effects on the water and energy flux analysis.

2.4. Calculations of hydrometeorological parameters

Hydrometeorological parameters were used to identify the reasons for seasonal and interannual variability in ET. The parameters selected were G_s, the Priestley–Taylor coefficient (α; Priestley and Taylor, 1972), and the Bowen ratio (β; Bowen, 1926).

G_s was calculated by inverting the Penman–Monteith equation

$$G_s = \frac{\gamma LEG_a}{\Delta(R_n - G) + \rho c_p VPD - LE(\Delta + \gamma)} \quad (1)$$

where G_s is surface conductance (m s^{-1}), γ is the psychrometric constant (kPa °C^{-1}), LE is latent heat flux measured by EC, G_a is aerodynamic conductance (m s^{-1}), Δ is the slope of the saturation vapor pressure versus temperature curve (kPa °C^{-1}), R_n is net radiation at the study area (W m^{-2}), G is the heat energy density into the soil (soil heat flux, W m^{-2}), ρ is air density (1.2 kg m^{-3}), c_p is the specific heat of the air (1004.7 J kg^{-1} K^{-1}), and VPD is air vapor pressure deficit (kPa) at the observation height. Note: outlier G_s values were not used when analyzing the relationship between G_s and other parameters.

The calculation of aerodynamic conductance (G_a) can be calculated as (Paulson, 1970; Businger et al., 1971; Massman, 1992; Li et al., 2015):

$$G_a = \frac{k^2 W_s}{\left[\ln\left(\frac{z}{z_o}\right) - \psi_h\right]\left[\ln\left(\frac{z}{z_o}\right) - \psi_m\right]} \quad (2)$$

where W_s is average wind speed at height z (m s^{-1}); k is von Karman's constant, 0.41 (−); z is the reference height (m); d is the zero plane displacement height (m); z_o is roughness length of the crop relative to momentum transfer (m); ψ_h is the stability correction function for heat and water transfer; ψ_m is the stability correction function for momentum transfers.

The Priestley–Taylor coefficient (α), which is the ratio of measured ET (ET_a) to equilibrium evaporation (ET_{eq}), can determine whether atmospheric demand or surface moisture supply is the limiting factor. The calculation of ET_{eq} is as follows:

$$\lambda ET_{eq} = \frac{\Delta}{\Delta + \gamma}(R_n - G) \quad (3)$$

An $ET/ET_{eq} \geq 1$ indicates that available energy (R_n–G) is the main factor controlling ET due to sufficient soil water (McNaughton and Spriggs, 1986). In arid and semi-arid regions, this value is often less than 1. It is reasonable to use the ET/ET_{eq} ratio to compare different observational sites because the sites are normalized by equilibrium rates, mainly determined by R_n (Wilson and Baldocchi, 2000).

The Bowen ratio (β; Bowen, 1926), which is the ratio of sensible heat flux (H) to latent heat flux (LE), through its effect on the warming extent of available energy to the ecosystem land surface air, heavily influences the ecosystem microclimate and hydrological cycle at both regional and global scales (Tang et al., 2014). The Bowen ratio is calculated as

$$\beta = \frac{H}{LE} \quad (4)$$

2.5. Data analysis

Path analysis was conducted to analyze the individual effects of independent variables on dependent variables (Edwards and Lambert, 2007). It is widely used in multiple regression because it can exclude potential relationships between independent variables (Rodrigues et al., 2014). Although it is similar to multiple regression, path analysis can estimate the strength and relative importance of assumed causal relationships among variables. Path analysis is most effective in the absence of feedback and for evaluating data in which independence among variables is not certain, rendering more common multiple regression techniques inappropriate (Huxman et al., 2003; Zhuang et al., 2016). Similar studies have adopted this method to reveal the direct effects of microclimate meteorological (air temperature: T_{air}, net radiation: R_n, vapor pressure deficit: VPD, volumetric soil water content: VWC, wind speed: W_s and surface conductance: G_s) and biological (leaf area index: LAI) variables on ET. The standardized partial regression coefficient represents the direct effects of the meteorological and biological variables on ET(Eq. 5), and the sum of the standardized partial regression coefficients across each path is the indirect effect of the variable (Huxman et al., 2003; Rodrigues et al., 2014; Tian et al., 2016).

The path analysis of ET was conducted based on the followed equation:

$$ET = f(T_{air}, R_n, VPD, VWC, W_s, LAI, G_s). \quad (5)$$

Linear fitting was used to evaluate energy balance of the EC data and to analyze the relationship between measured ET and ET_{eq}. Nonlinear fitting was used to analyze the relationship between G_s and α.

All of the data analysis was performed using SPSS25.0 software.

3. Results

3.1. Meteorological information and energy balance closure

Studies have used the energy balance closure (calculated as linear regression analysis of available energy (R_n–G) and the sum of sensible and latent heat fluxes (H+LE)) to evaluate the quality of EC data (Wilson et al., 2002; Rodrigues et al., 2014). Based on the daily data without gap filling from June 2013 to June 2018, the slope between H+LE and R_n–G during the summer maize and winter wheat growing seasons was 0.79 and 0.87, respectively, with respective regression intercepts of 9.96 W m^{-2} and −1.48 W m^{-2}, and coefficients of determination (R^2) of 0.81 and 0.92 (Fig. 2). The results of the regression analysis are shown in Table 2. For the five-year study period, the slopes of the regression analysis ranged from 0.75 to 0.90 during the maize growing season and 0.70 to 0.91 during the wheat growing season, and the intercepts ranged from 3.40 to 13.22 W m^{-2} and –9.30 to 4.71 W m^{-2} for the maize and wheat growing seasons, respectively, thus indicating that some heat fluxes were not accounted for by the EC system.

Even though many long-term flux observations based on the EC technique have been conducted worldwide, the reasons for residual energy and lack of energy balance closure are not fully understood (Foken, 2008; Widmoser and Wohlfahrt, 2018). Likewise, we found it difficult to identify the main factors that caused the energy imbalance in this agroecosystem. Measurement errors from the instruments (e.g., soil heat flux plates and EC system), sensible heat advection, energy consumed by photosynthesis, and energy storage in the surface soil layer and crop canopy could affect the energy balance (Li and Yu, 2007). Meyers and Hollinger (2004) reported that canopy and photosynthetic storage accounted for nearly 14% and 8% of R_n in maize and soybean (*Glycine max* L.), respectively. It is likely that the difference in canopy heat storage was the primary factor for the different energy balance closure between maize and wheat in our study. Based on the data from FLUXNET (Baldocchi et al., 2001), the slopes of the energy balance closure ranged from 0.53 to 0.99 (mean = 0.79 ± 0.01) and intercept values ranged from –32.9 to 36.9 W m^{-2} (mean = 3.7 ± 2.0) (Wilson et al., 2002). For ChinaFLUX sites, the slopes ranged from 0.49 to 0.81 (mean = 0.67) and intercept values ranged from 10.8 to 79.9 W m^{-2} (mean = 28.9) (Li, 2005). The slope and intercept in the current study

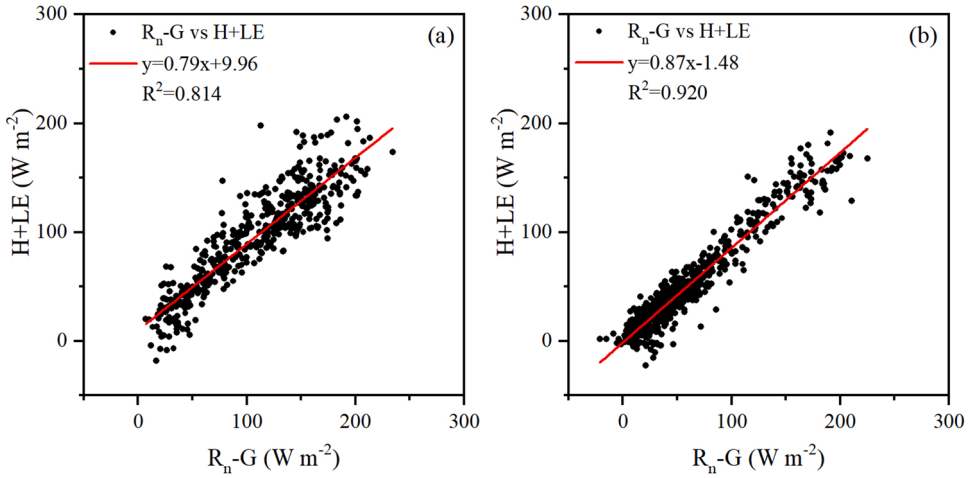

Fig. 2. Daily energy balance closure for latent plus sensible heat fluxes (LE+H) versus net radiation minus soil heat flux (R_n–G) during the (a) summer maize and (b) winter wheat growing seasons (2013–2018) near Yangling, China.

Table 2
Energy balance analysis of latent heat plus sensible heat fluxes (LE + H) versus available energy (R_n–G) in the 2013–2018 summer maize and winter wheat growing seasons in Yangling, China.

	Summer maize			Winter wheat		
Year	Slope	Intercept	R^2	Slope	Intercept	R^2
2013	0.76	13.22	0.75	0.91	–3.00	0.94
2014	0.90	3.40	0.81	0.89	–2.10	0.92
2015	0.75	12.10	0.85	0.83	–9.30	0.74
2016	0.80	8.84	0.82	0.70	1.00	0.92
2017	0.78	4.92	0.88	0.83	4.71	0.96
5 years	0.79	9.96	0.81	0.87	–1.48	0.92

Note: R_n is net radiation; G is soil heat flux.

were comparable with these studies. Twine et al. (2000) introduced the Bowen ratio method for overcoming the energy imbalance issue, which assumes that the Bowen ratio can be measured accurately and forces the energy closure. Using the corrected long-term quality-assured observed data, we analyzed annual and interannual variation in energy fluxes in the studied ecosystem.

During the observation period, solar radiation (R_g) and VPD ranged from 0.2 to 34.4 MJ m^{-2} d^{-1} and 0 to 2.98 kPa, respectively; both of which had typical seasonal variation (Fig. 3a). The mean annual temperature over the five years ranged from 13.7 to 14.5 °C (mean 12.9 °C from 1990 to 2008). The maximum temperature during the observation period was 42.2 °C, and the minimum temperature was −9.3 °C (Fig. 3b). The average annual precipitation was 599 mm, slightly below the 1990–2008 average of 630 mm. Most of the rainfall occurred from April to October during the maize and wheat growing seasons. There was relatively low precipitation from November to March when winter wheat was dormant. Total precipitation ranged from 210 to 394 mm during the maize growing seasons, and 202 to 385 mm during the wheat growing seasons (Fig. 3c). Although the temporal variability of precipitation was substantial, VWC remained relatively high during the crop growing seasons with the use of sufficient irrigation (Fig. 3c). LAI peaked twice each year due to the winter wheat/summer maize rotation (Fig. 3d). After the wheat was planted around 20 October, LAI increased slightly with emergence and early season growth, decreased when winter wheat was dormant, increased sharply in early March when regrowth began—peaking in late April/early May (4.04–4.93 m^2 m^{-2})—before rapidly decreasing until harvest. In the summer maize cropping season, LAI peaked in early August (3.59–5.31 m^2 m^{-2}) before decreasing as maize progressed to physiological maturity in late September.

3.2. Hydrometeorological parameters

Seasonal patterns of daily α, ET_a, ET_{eq}, and G_s for this ecosystem were similar to those previously reported (Lei and Yang, 2010; Shen et al., 2013; Suyker and Verma, 2008). Generally, α followed a clear annual cycle during the measurement period (Fig. 4a). The α value peaked during winter when wheat was dormant, indicating that sensible heat advection in winter significantly enhances ET. Annual average values of α over the five years of the study (Table 1) ranged from 1.00 to 1.13, thus indicating that α is a relatively stable parameter for estimating actual annual ET totals in this region. The average α values during the five wheat growing seasons ranged from 1.17 to 1.37 (Table 1). These values were higher than the average α values during the five maize growing seasons, which ranged from 0.82 to 1.00 (Table 1), which indicated that the water consumption capacity of wheat is greater than that of maize under the same radiative condition.

The seasonal variation in daily ET, as well as daily equilibrium evaporation during the five years of the study, are shown in Fig. 4b. Because winter wheat was planted in mid-October, ET gradually increased from about 0.5 to 2.5 mm d^{-1} from emergence to early canopy development in November. During the winter dormancy period (December to January), ET reached minimum values due to both minimum equilibrium evaporation values and no transpiration from wheat. Subsequently, daily ET values were consistent with ET_{eq} until late May when winter wheat began to senesce. As shown in Fig. 4b, ET was relatively low in June (~2.0 mm d^{-1}) despite the high equilibrium evaporation because of the crop rotation used. As a result of the rapid maize growth from late June to August, ET rapidly increased during this period before rapidly decreasing from late August as summer maize matured and ET_{eq} decreased. The daily ET of wheat reached maximum values between 5.5 and 6.0 mm d^{-1}, whereas maize reached maximum daily ET values between 5.2 and 6.7 mm d^{-1}. Because the peak ET_{eq} for maize was slightly higher than that of wheat, maize had higher ET_a during times of peak ET_{eq} (~6.5 mm d^{-1}) than wheat. During the wheat growing seasons, equilibrium evaporation (ET_{eq}) explained 84.6% of the seasonal variability in daily ET. During the maize growing seasons, ET_{eq} explained 82.6% of the seasonal variability in daily ET. The slope of the relationship between ET_a and ET_{eq} was 0.93 and 1.04 for the maize and wheat growing seasons, respectively (Fig. 5), and this can likely be attributed to the greater water use efficiency of C4 maize than C3 wheat (Tong et al., 2009). A similar result was reported by Lei and Yang (2010) in a maize/wheat rotation system in the North China Plain. The scatter of data points around the regression lines in Fig. 5 indicates that other environmental factors are influencing actual ET. The outlier values usually occurred between the wheat and maize rotation phases when

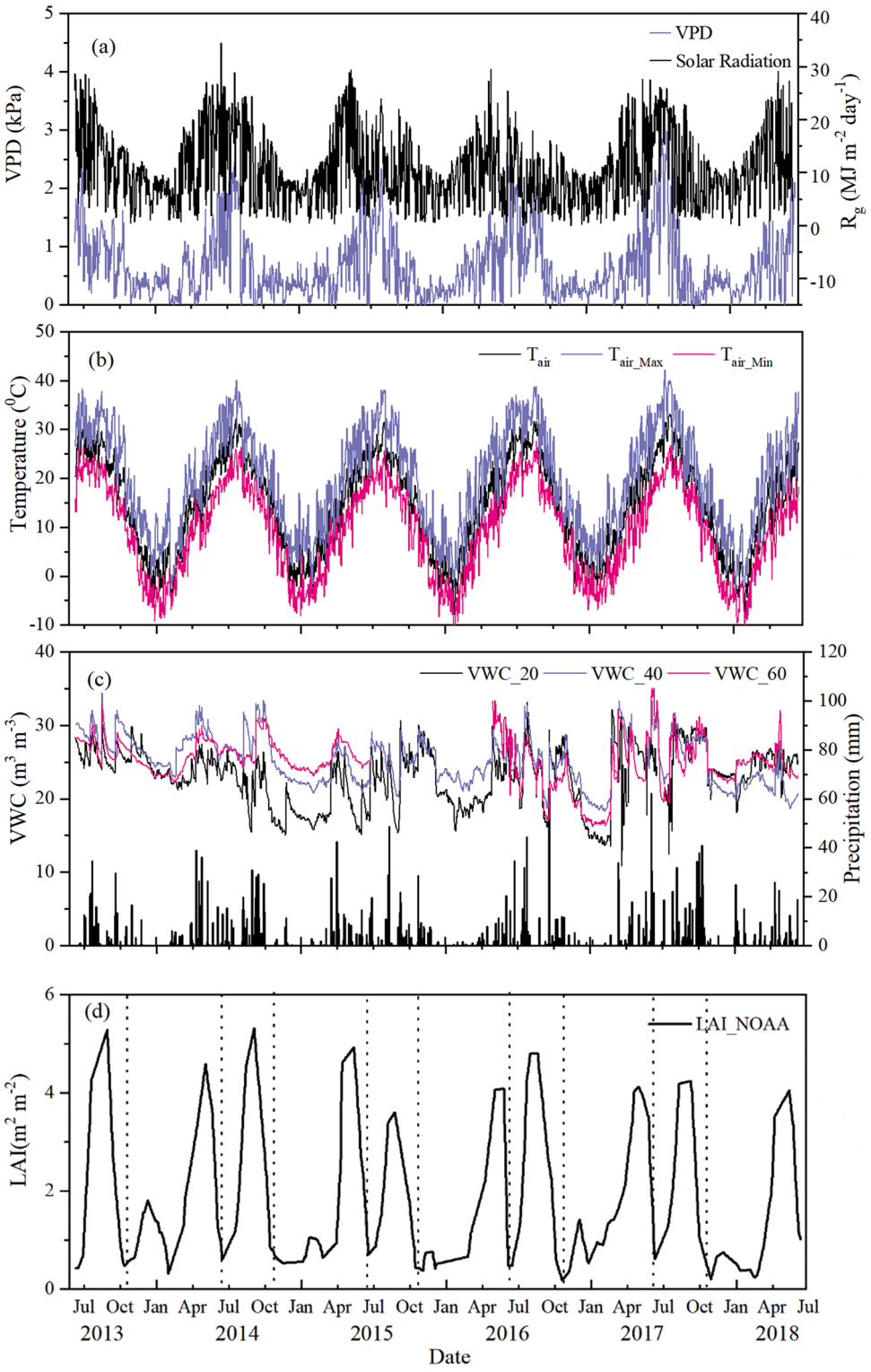

Fig. 3. Seasonal and inter-annual variability in environmental and biological factors from 2013 to 2018 near Yangling, China. (a) Solar radiation (R_g) and vapor pressure deficit (VPD); (b) daily mean air temperature (T_{air}), maximum air temperature (T_{air_Max}), and minimum air temperature (T_{air_Min}); (c) volumetric soil water content at depths of 20, 40, and 60 cm (VWC_20 cm, VWC_40 cm, and VWC_60 cm) and daily precipitation (P); and (d) leaf area index (LAI).

LAI was low but ET_{eq} was high.

Surface conductance has been used as a parameter to reflect biological factors controlling seasonal variation in ET (Baldocchi et al., 2004). Annual and interannual variation in daytime G_s is shown in Fig. 4d. As crop production moved between wheat and maize phases, G_s decreased as LAI reached the minimum values. Daytime G_s was about 1 mm s^{-1} during the wheat dormancy period in winter, and then increasing to 25–29 mm s^{-1} when LAI reached maximum values in April. In the maize growing season, peak G_s values reached 13–17 mm s^{-1} during vigorous growth in August. Maximum G_s values occurred when wheat and maize were actively growing. The winter wheat growing season produced around two times higher average surface conductance

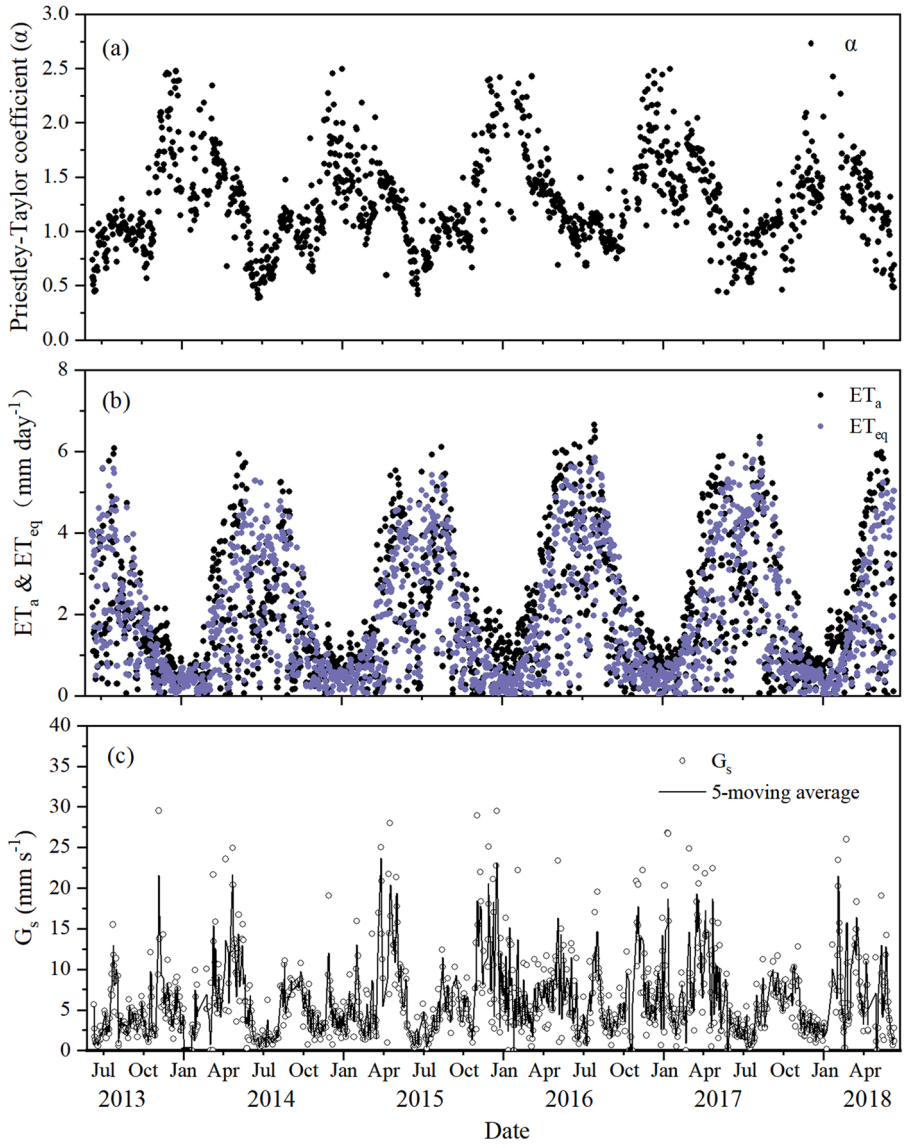

Fig. 4. Seasonal and inter-annual variability in daily surface parameters from 2013 to 2018 in a summer maize–winter wheat cropping system in Yangling, China. (a) Priestley–Taylor coefficient (α), (b) equilibrium evaporation (ET_{eq}) and actual evapotranspiration (ET_a), and (c) surface conductance (G_s).

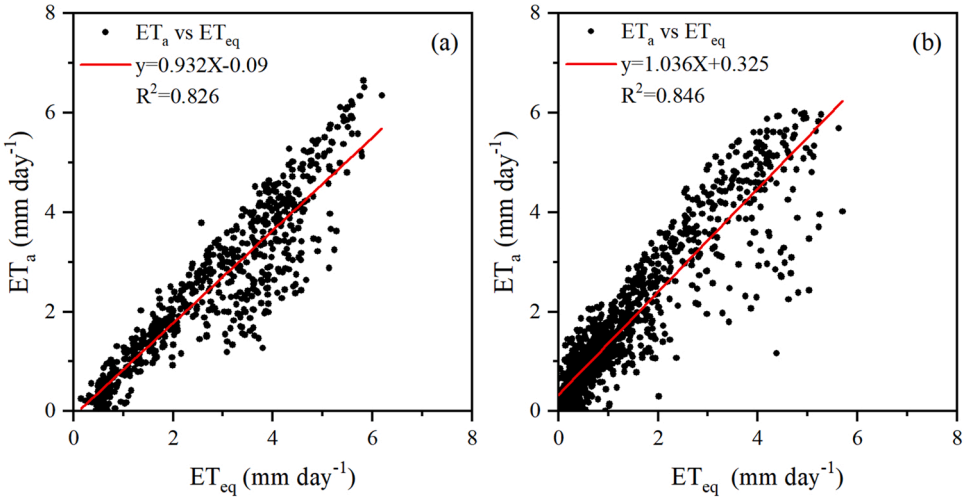

Fig. 5. Relationship between daily actual evapotranspiration (ET_a) and equilibrium evaporation (ET_{eq}) during the (a) maize and (b) wheat growing seasons near Yangling, China. Additional environmental factors likely caused the scatter in ET_a around the regression lines.

than the maize growing season, which agrees with the two or more times higher G_s values observed in a fully developed wheat field (C3 plant) than a maize field (C4 plant) (Baldocchi, 1994).

3.3. Energy partitioning and Bowen ratio variations

Seasonal variability in daily R_n, H, LE, and G during the five years of the experiment are shown in Fig. 6. The maximum daily LE (between 150 and 200 W m^{-2}) usually occurred mid-season during May and August, respectively, and corresponded with maximum leaf area development (Fig. 6a). The first peak in daily H values occurred in June to early July between wheat senescence and rapid maize development. The second, lower peak occurred in October between maize senescence and early wheat development (Fig. 6a). We expect that this difference between locations is attributable to the lower latitude of our experimental site than the North China Plain, resulting in relatively higher R_n when maize matured.

The H decreased rapidly following crop emergence each year. During the rapid growth of wheat, daily H values were near zero. However, H rarely reached zero in the rapid growth period of summer maize. The ratios of heat fluxes to available energy (LE/(R_n–G), H/(R_n–G)) are shown in Fig. 6b to verify the relationship between seasonal variations in energy partitioning and crop phenology. Three peaks of LE/(R_n–G) were observed in each crop year. During the wheat growing season, peak values usually occurred in November (due to the emergence of wheat) and late April/early May (full canopy development and maximum LAI), and August (maximum LAI during the maize growing season). During the wheat growing season, LE/(R_n–G) ranged from 0.30 to 0.60 during the dormant season and 0.90 to 0.95 when maximum LAI was reached. As wheat approached maturity, LE/(R_n–G) sharply declined to approximately 0.25. During the maize growing season, LE/(R_n–G) peaked at approximately 0.8–0.9, which was lower than the values observed in the winter wheat growing season. The values for H/(R_n–G) followed the opposite pattern to that seen for canopy development (Fig. 6b).

The diurnal variations in energy fluxes (R_n, LE, H, and G) each month, averaged from 2013 to 2018, are shown in Fig. 7. All energy components followed familiar bell-shaped variation each day. The figure also shows that the energy fluxes exhibited clear seasonal variability with significant differences due to the development and senescence periods of the two crops. Midday R_n increased from 209 W m^{-2} in January to 513 W m^{-2} in July, with a slight decline from the peak value in June due to increased cloudiness associated with the rainy season. R_n

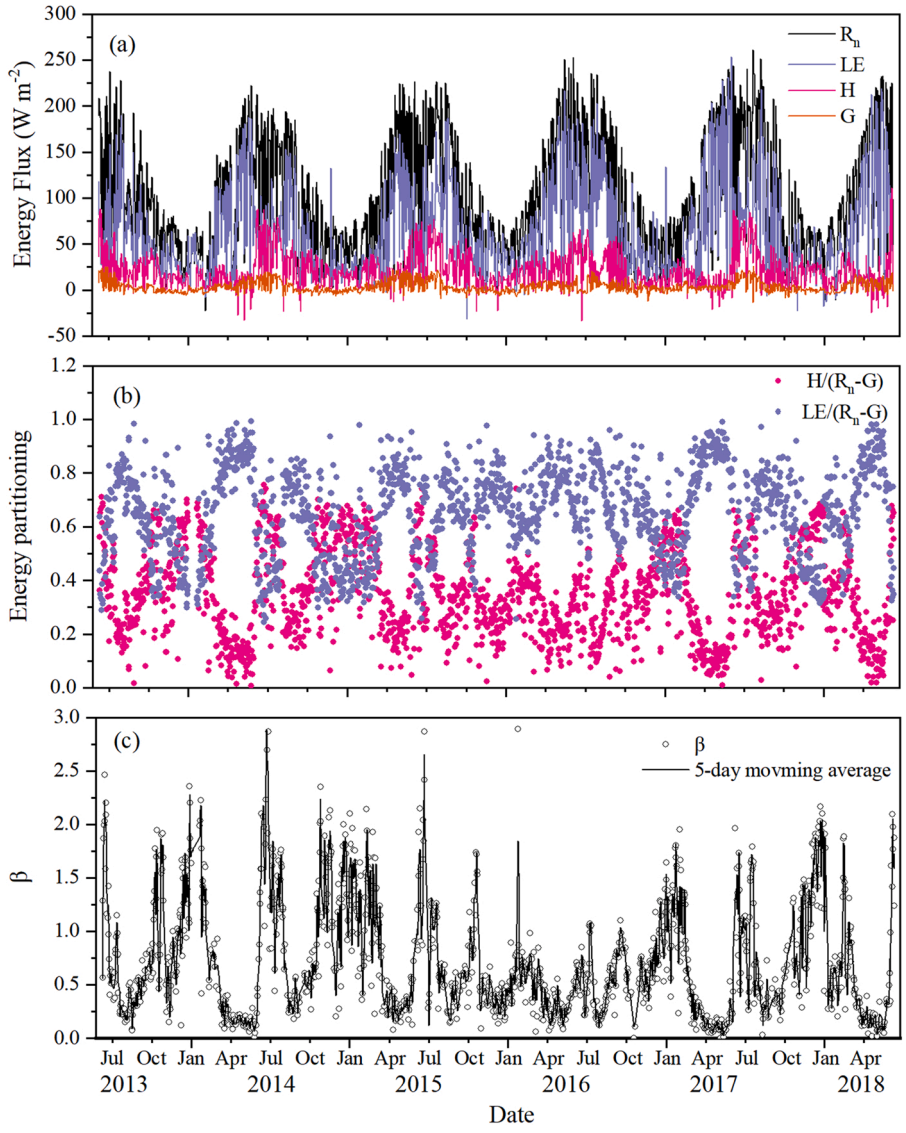

Fig. 6. Seasonal and inter-annual variability in daily (a) average net radiation (R_n), soil heat flux (G), sensible heat flux (H), and latent heat flux (LE); (b) energy partitioning; and (c) Bowen ratio (β) from 2013 to 2018 near Yangling, China.

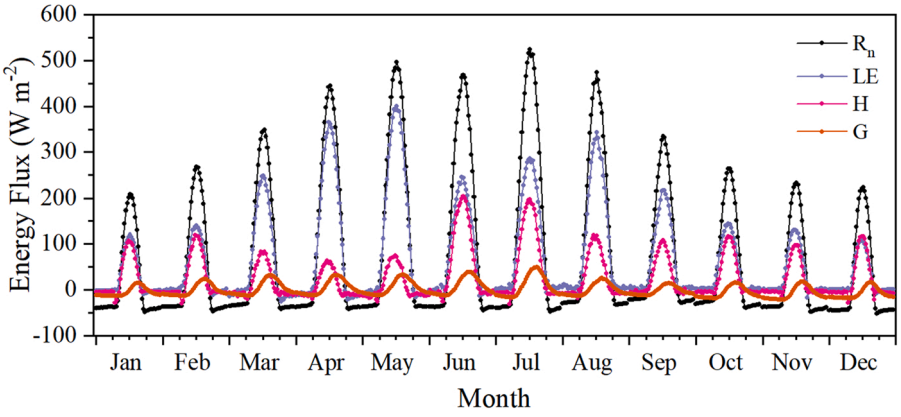

Fig. 7. Average diurnal time course of net radiation (R_n), latent heat flux (LE), sensible heat flux (H), and soil heat flux (G) over a summer maize–winter wheat field near Yangling, China. Data points are 30-min averages computed from data collected each day of a given month from 2013 to 2018.

decreased to 223 W m^{-2} in December. LE peaked in May (400 W m^{-2}) (maximum wheat leaf area) and August (442 W m^{-2}) (maximum maize leaf area). High H values occurred from October to February when LAI values were low, at which time H and LE were nearly equal. Wheat leaf area increased rapidly in March, with a subsequent decline in H. G only consumed a small fraction of R_n, and showed diurnal hysteresis, peaking approximately 3 h later than the other three energy components.

Annual variability in the daily Bowen ratio (Fig. 6c) was large during the two crop phases in a given year, as well as the winter wheat dormancy period, with maximum values ranging from about 1.5 to 2.9. However, β was relatively low when soil moisture was very high (e.g., June 2016 and October 2016 when the VWC was high). As the maize and wheat canopies developed fully, the β values decreased to relatively stable, low values (0.1–0.3), with mean values of 0.50 in the wheat growing season and 0.59 in the maize growing season.

3.4. Environmental and biological controls on evapotranspiration

Path analysis was used to determine the importance of daily meteorological, hydrological, and biological variables (R_n, G_s, VPD, LAI, T_{air}, and VWC) on ET during the maize and wheat growing seasons (Fig. 9 and Table 3). As the figures shown, R_n was the primary direct factor controlling ET in both the maize and wheat growing seasons and the direct path coefficient of R_n to ET was 0.730 and 0.718 for maize and wheat season, respectively. Besides R_n, G_s was another main direct factor that controlling ET. The direct path coefficient of G_s to ET was 0.345 and 0.212 for maize and wheat season, respectively. The direct path coefficient of VPD to maize ET was 0.121, which was less sensitive when compared with wheat ET. Both maize and wheat ET were directly affected by LAI, but the direct path coefficient of LAI to wheat ET (0.082) was lower than to maize ET (0.199). As shown in Fig. 9, only wheat ET was affected by VWC and T_{air}, indicating that wheat ET is prone to be affected by the soil water content during the growing season, although the crop was well watered. The maize season G_s was more sensitive to VPD than wheat season G_s, which results in a greater indirect effect of VPD through G_s on ET. Although the maize ET was not directly affected by VWC, there was a relatively higher indirect effect of VWC through G_s on ET.

Table 3
Path coefficients of the direct and indirect effects of daily net radiation (R_n), vapor pressure deficit (VPD), surface conductance (G_s), leaf area index (LAI), air temperature (T_{air}) and volumetric water content (VWC) on evapotranspiration (ET) for the maize and wheat seasons.

	Maize ET		Wheat ET	
	Direct	Indirect	Direct	Indirect
R_n	0.73	0.06	0.718	0.117
VPD	0.121	–0.187	0.151	-0.008
G_s	0.345	NS	0.212	NS
LAI	0.199	0.158	0.082	0.021
T_{air}	NS	NS	0.042	NS
VWC	NS	0.113	0.065	0.079

The direct effects of meteorological, hydrological, and biological factors on ET are shown by month in Fig. 10. Similar to the results shown for the growing season analysis (Fig. 9), R_n was the primary direct path for ET, with direct path coefficients was around 0.75 from March to September, evidenced by the nearly synchronized variations in daily averages of R_n and ET. The controlling power of VPD and G_s on ET was weaker than the effect of R_n on ET, whereas the effect of VPD and G_s on ET was also strong in some specific months. The relatively lower path coefficients of G_s on ET corresponded with the higher LAI in wheat and maize season. These results are consistent with the results of the seasonal-scale analysis. VWC generally significantly affected ET in November, December, and March, while wheat was experiencing dormancy, the soil had relatively low water content, and ET was mainly composed of soil evaporation. ET was not directly affected by T_{air} in most months. A positive direct effect of LAI on ET occurred in May, June, August, and October, and corresponded with periods of the large variability in LAI.

The indirect effects of VPD, LAI, VWC, and R_n through G_s on ET are shown by month in Fig. 11. VPD, which can significantly affect G_s, was the primary indirect controlling factor of ET. The most significant negative indirect effect of VPD occurred in July, which corresponded with the highest VPD values. At the same time, the highest positive indirect effect of LAI on ET was also founded in July, which corresponded with the rapid growth period of maize. The indirect effects of R_n on ET through G_s were relatively low in each month. Although VWC cannot directly affect ET in July, it can indirectly affect ET by affecting G_s. It is consistent with the results of the seasonal-scale analysis.

4. Discussion

4.1. Environmental and biological controls on evapotranspiration

Plant water use is influenced by both species type and the prevailing environmental conditions during the growing season (Xu et al., 2018). The maximum G_s values for maize and wheat (19.5–29.5 mm s^{-1}) (Fig. 4c) were comparable with those reported by Lei and Yang (2010) in a similar rotation cropland in the North China Plain (15–30 mm s^{-1}), Ding et al. (2013) in maize fields in an arid region (20 mm s^{-1}), and Tian et al. (2016) in cotton fields (13–20 mm s^{-1}), lower than those reported by Suyker and Verma (2008) in maize and soybean fields in Nebraska, USA (30–40 mm s^{-1}). ET increases with G_s, but this relationship does not continue when G_s is higher than a threshold value (Fig. 8). There are

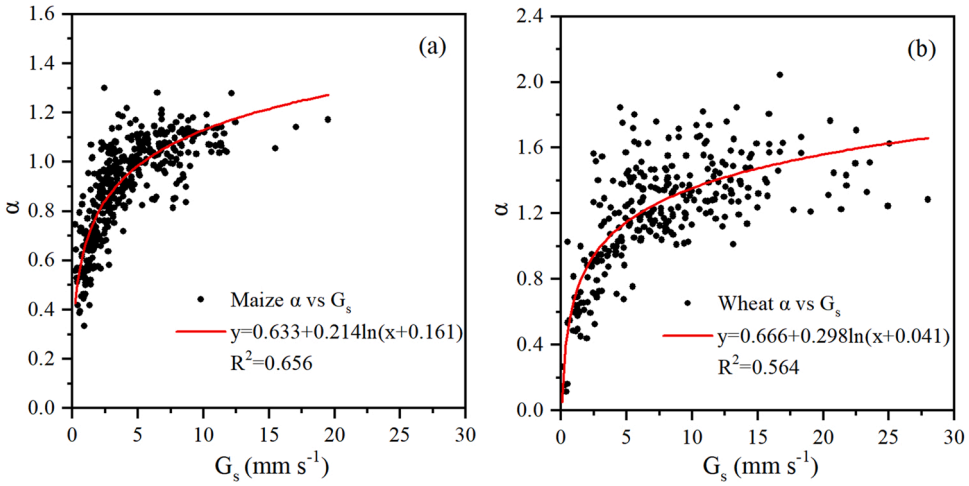

Fig. 8. Relationship between Priestley–Taylor coefficient (α) and canopy conductance (G_c) during the (a) maize and (b) wheat growing seasons (after the wheat returning green stage) near Yangling, China.

numerous previous studies have demonstrated that the R_n is the primary driver of ET. But the effect of the other environmental and biological factors varies with climate type and land surface. Generally, the values of G_s reflect the effects of biological factors on the seasonal variation in ET, and the values of ET_{eq} can reflect the effect of environmental factors on seasonal variation in ET. However, G_s was also affected by VPD and soil water content. A study conducted by McNaughton and Spriggs (1986) reported that α was sensitive to G_s when G_s was less than a threshold value. Suyker and Verma (2008) reported a consistent threshold of G_s in a maize field. The threshold G_s at our site (10 mm s^{-1}) was lower than the threshold G_s values reported by Lei and Yang (2010) in a wheat/maize rotation (15–20 mm s^{-1}), Ding et al. (2013) in a maize field (20 mm s^{-1}), and Suyker and Verma (2008) in a maize and soybean rotation (10–15 mm s^{-1}), but slightly higher than the threshold G_s value reported by Tian et al. (2016) in a cotton field in northwest China (8 mm s^{-1}). The other studies have also reported this threshold phenomenon, but the threshold varies with ecosystems and climates (Ryu et al., 2008; Zha et al., 2013; Ma et al., 2015; Tan et al., 2019; Marques et al., 2020). For croplands with a large amount of irrigation, such as the wheat/maize rotation cropland in the North China Plain, the ET was mainly controlled by R_n. Therefore, the α values could increase until G_s reached a relatively high value. For the Yangling site, due to the Rn was significantly higher than that of Weishan and Luancheng, the controlling effect of R_n was lower than other mentioned sites. Thus, the threshold of G_s was lower that reported by Lei and Yang (2010), Ding et al. (2013), and Suyker and Verma (2008). The ET in the cotton field was mainly controlled by soil moisture due to the sufficient R_n. It results that the threshold value of G_s of the cotton was slightly lower than that of the maize at Yangling.

The VPD had two paths that can affect ET. On the one hand, a higher VPD will result in a higher ET as it reflects a high vapor pressure difference between air and stomatal or soil pores, which can enhance water vapor flow through stomata or the soil surface. On the other hand, the increasing VPD will reduce the stomatal aperture, which will increase stomatal resistance and reduce ET and was demonstrated in previous studies (Lei and Yang, 2010; Tian et al., 2016; Suyker et al., 2008; Gong et al., 2020; Marques et al., 2020). This study quantified the direct and indirect effects of VPD on ET. The increased flow through stomata as a function of VPD would be compensated for by reductions in stomatal aperture and increased flow rate through stomata. As the path analysis of ET showed, the maize season G_s was more sensitive to VPD than wheat season G_s, which indicates that the higher VPD in summer can significantly and indirectly reduced ET. This was due to decreasing stomatal conductance as VPD increased (Rodrigues et al., 2014). These results are consistent with those in a maize ecosystem (Ding et al., 2015).

The direct effect of LAI was relatively small in the monthly analysis; the reason is that the variation of LAI is small except for the rapid growth period of crop and the rotation period. VWC had two paths that can indirectly affect ET. In the seasonal and interannual scale, VWC can affect the development of LAI. Furthermore, VWC can directly and positively affect G_s by decrease soil surface resistance and stomatal resistance, then increasing soil evaporation and transpiration. Although the crop was rarely suffering moderate or severe water stress due to irrigation, VWC was relatively low due to lack of irrigation and the ET was mainly made up of soil evaporation when the wheat going into dormancy. Thus, the direct effect of VWC can be found in November and December. Then, the different effects of VWC for maize and season in Fig. 9 can be explained.

In addition, there was a different effect of T_{air} for the maize and wheat seasons. In the monthly path analysis, ET was directly affected by T_{air} in October, November, and February. The air temperature in October, November, and February can significantly affect the emergency, dormancy, and returning green stages of winter wheat. The transpiration of wheat will stop when wheat is experiencing dormancy and will increase when the wheat enters the returning green stage. In warmer winter, for wheat, the dormancy date will be delayed and the returning green stage will advance, which would increase ET, although the effect was relatively low. In summer, as the air temperature was high, and the phenology of maize was usually controlled by soil water content rather than the air temperature. Therefore, the significant direct effect of T_{air} was not founded during the maize season. The indirect effect of soil moisture on ET through G_s was relatively low for both wheat and maize because G_s was less affected by soil moisture when soil moisture was relatively high (Xu et al., 2018). The reason why VPD has a high indirect effect on ET through G_s in the monthly analysis is that increases in vapor flow through stomata as a function of vapor pressure deficit would be compensated for by reductions in stomatal aperture, which was consistent with the results of the seasonal analysis. Figs. 9–11 illustrate that path analysis can identify the primary factors controlling ET.

4.2. *Bowen ratio in various ecosystems of China*

The seasonal variation in daily β in the winter wheat and summer maize rotation agroecosystem near Yangling, China followed the pattern of a double U-shaped curve, with minimum values occurring in May and August each year (Fig. 6c). During the study period, the mean values of β for the maize growing season, the wheat growing season, and annually

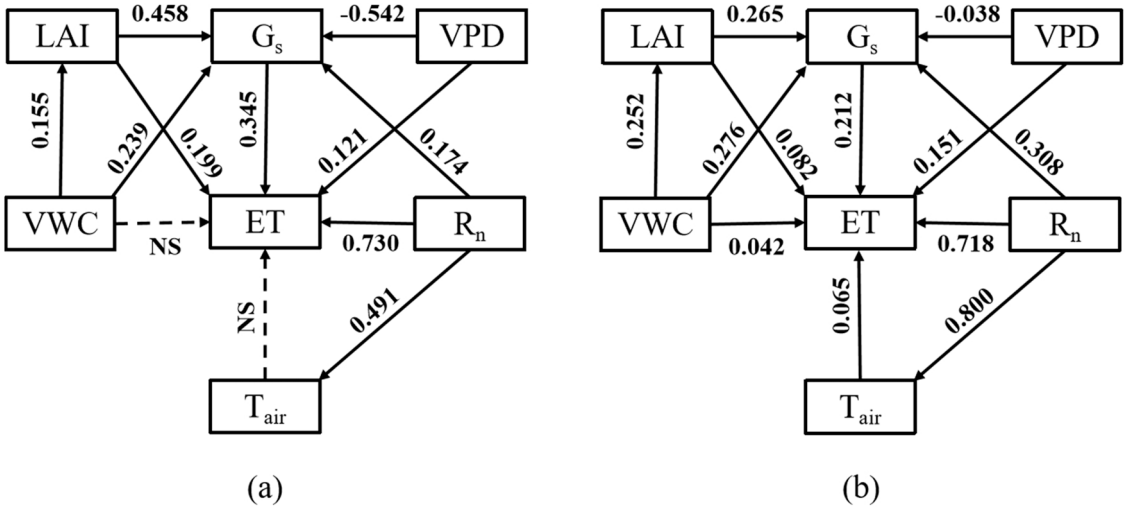

Fig. 9. Path analysis illustrating the relative importance of the eco-hydrological variables net radiation (R_n), air temperature (T_{air}), vapor pressure deficit (VPD), volumetric soil water content (VWC), and leaf area index (LAI) on evapotranspiration (ET) during the 2013–2018 (a) maize and (b) wheat growing seasons. Paths that were not significant at $P < 0.05$ are indicated as 'NS'; all other paths were significant at $P < 0.05$.

were 0.59, 0.50, and 0.53, respectively (Table 4). These values differ from those reported in other ecosystems, such as spring maize, grassland, and forest (Gao et al., 2018; Li et al., 2006; Wilson and Baldocchi, 2000). As Table 3 shows, the β values during both the maize and wheat growing seasons on the Guanzhong Plain were higher than those reported on the North China Plain (Lei and Yang, 2010). This may be attributed to the R_n of Yangling was much higher than that of Weishan and Luancheng. Owing to irrigation, the annual ET of this study was higher than that of a grassland on the Loess Plateau. This leads to a much lower β compared to the grassland site (Ping et al., 2018). This indicates that a high water-consuming agroecosystem can significantly change its energy partitioning.

Some periods of negative sensible heat flux were measured during the dormancy period of winter wheat in winter, which can be attributed to the advection of H (Prueger et al., 1996), and indicates that H can provide energy for evapotranspiration during the dormancy period (Lei and Yang, 2010). Many studies have reported that changes in actual evapotranspiration are mainly affected by changes in precipitation rather than equilibrium evaporation in regions that are prone to drought (such as the Guanzhong Plain), but the reverse is true in humid regions (Yang et al., 2007). However, in agroecosystem studied here, the variability in actual evapotranspiration was primarily explained by ET_{eq}, and no significant relationship was found between ET and precipitation. This result indicates that the patterns of ET and energy partitioning can be changed by human activity (e.g., large amounts of irrigation). Large spatial scale irrigation results in sensible heat advection, which subsequently affects local energy partitioning and the water cycle.

On an annual basis, LE consumed a large proportion of net radiation (62.6%), which was slightly higher than those reported for maize and soybean fields in Nebraska, USA (60%; Suyker and Verma, 2008), maize/wheat agroecosystems in the North China Plain (59%; Lei and Yang, 2010; Shen et al., 2013), and a temperate mixed forest ecosystem in Changbai Mountain (52%; Wu et al., 2007), but much higher that reported for a grassland ecosystem in the Tibetan region (24%; Gu et al., 2005). The mean value of daytime LE/(R_n–G) was about 66.9% in the wheat growing season and 63.5% in the summer maize growing season, indicating that wheat consumed more water than maize for a given amount of energy.

4.3. Annual evapotranspiration for maize and wheat in various regions of China

Two of the most important grain crops worldwide—maize and wheat—are widely cultivated in North China. It is vital to understand the differences in timing and amount of water use for these two crops in different regions. Therefore, ET for maize and wheat between different regions in North China was compared, and the data is presented in Table 5. Summer maize generally has a lower ET than that of spring maize due to its shorter growing season. We did not find a significant relationship between ET and precipitation as the irrigation mitigated the effects of low precipitation. A comparison of the three main summer maize planting areas in China (Weishan, Luancheng, and Yangling) (Lei and Yang, 2010; Shen et al., 2013) revealed that summer maize in Yangling consumes more water than the other two locations. The reason is that Yangling has higher R_n and VPD than Weishan and Luancheng. Yangling also had slightly lower winter wheat ET than Luancheng and slightly higher winter wheat ET than Weishan, thus indicating that sufficient irrigation can change the pattern of water and energy partitioning, relative to semi-arid and humid regions. In addition, irrigated cropland in semi-arid regions not only experiences lower precipitation than semi-humid regions but also higher evaporative demand.

5. Conclusion

EC observations of water and energy fluxes with good quality were made, and path analysis of ET with meteorological, hydrological, and biological factors was conducted in a typical irrigated winter wheat/summer maize rotation field in the Guanzhong Plain from June 2013 to June 2018. The total ET for each crop year was 645, 627, 753, 775, and 739 mm from June 2013 to June 2018. Average total evapotranspiration was 310 mm and 398 mm for the maize and wheat growing seasons, respectively. For both crops, ET increased rapidly with rapid canopy development, reaching peak values when the canopy was fully developed. The ET decreased as the canopy senesced. G_s reached 19.5 and 29.5 mm s^{-1} in the maize and wheat growing seasons, respectively. For both maize and wheat, daily β values were between 0.1 and 0.2 when LAI reached maximum values and ranged from 1.5 to 2.9 during the rotation period. The average β value in the five-year study was 0.59 for maize and 0.53 for wheat. R_n was the primary controlling factor of ET for both maize and wheat season. Also, G_s was another controlling factor that had more controlling power in maize season than in wheat season. VPD had a significant positive and direct effect on ET for both wheat and maize season, whereas it had a significant negative and indirect effect on ET through G_s in the maize season. VWC and T_{air} only directly affect the wheat ET. In addition, VWC had two significant paths that can indirectly affect ET through LAI and G_s. The understanding of the controlling

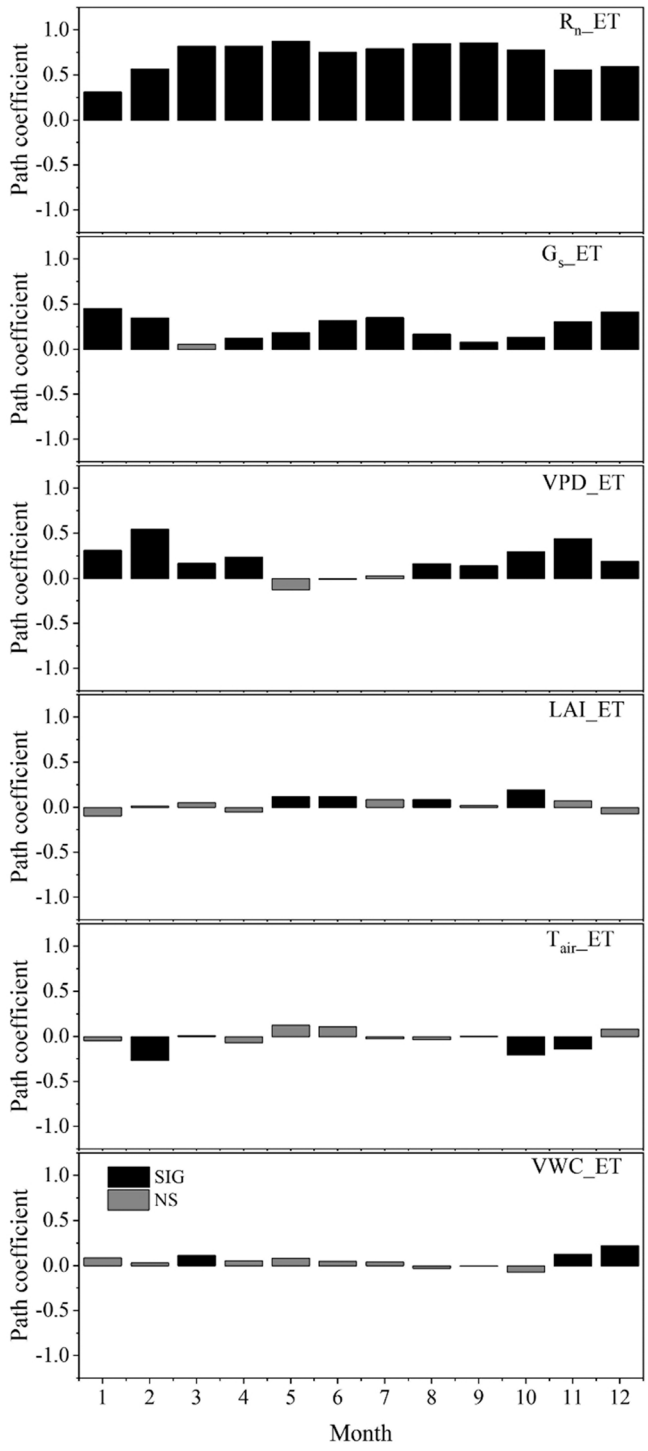

Fig. 10. Path analysis coefficients illustrating the direct effects of net radiation (R_n), surface conductance (G_s), vapor pressure deficit (VPD), leaf area index (LAI), air temperature (T_{air}), and volumetric soil water content (VWC) on evapotranspiration (ET) each month in Yangling, China. Black bars indicate significant path coefficients ($P < 0.05$) and gray bars indicate nonsignificant path coefficients.

factors of ET provides the theoretical basis for quantifying crop water requirements and improving water use efficiency.

Declaration of Competing Interest

The authors declare that they have no known competing financial

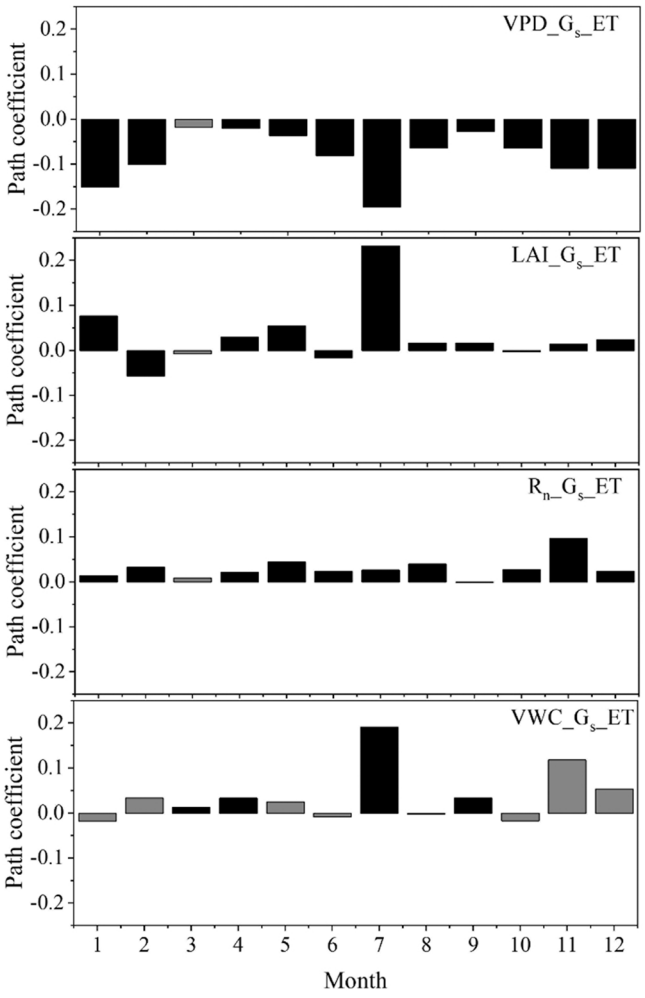

Fig. 11. The indirect effects of vapor pressure deficit (VPD), leaf area index (LAI), net radiation (R_n) and volumetric soil water content (VWC) through surface conductance (G_s) on evapotranspiration (ET) each month in Yangling, China. Black bars indicate significant path coefficients ($P < 0.05$) and gray bars indicate nonsignificant path coefficients. (VPD_G_s_ET means the indirect effect of VPD through G_s on ET).

Table 4
Review of average daily Bowen ratio (β) during the maize and wheat growing seasons at different sites in China. P is total precipitation during the indicated period.

Vegetation	Period	P	β	Reference
Maize in Guanzhong Plain	Jun 10–Oct 10, 2013–2018	311	0.59	This study
Maize in Luancheng	Late June to early October	301–417	0.28–0.47	(Lei and Yang, 2010)
Maize in Weishan	Late June to early October	215–386	0.37–0.48	Shen et al. (2013)
Wheat in Guanzhong Plain	Oct 10–Jun 10, 2013–2018	288	0.50	This study
Wheat in Luancheng	Late October to early June	70–197	0.16–0.23	(Lei and Yang, 2010)
Wheat in Weishan	Late October to early June	124–236	0.19–0.26	Shen et al. (2013)

Table 5
Annual evapotranspiration (ET) for summer maize, spring maize, and winter wheat in various regions of China varying in incoming net radiation (R_n), vapor pressure deficit (VPD), and precipitation (P).

Crop	Location	R_n (MJ m^{-2})	VPD (kPa)	P (mm)	Year	Time	ET (mm)	Reference
Summer maize	Yangling, Shannxi	1256	1.02	210–394	2013–2018	Mid June to early October	259–372	This study
	Weishan, Shandong	999–1046	0.690–0.853	215–366	2005–2008	Late June to early October	198–234	(Lei and Yang, 2010)
	Luancheng, Hebei	957–1025	NA	289–417	2008–2011	Late June to early October	239–300	Shen et al. (2013)
Spring maize	Shouyang, Shanxi	1752	NA	337–400	2015–2016	May 1 to October 10	338–350	Gao et al. (2018)
	Harbin, Heilongjiang	NA	NA	251–442	2014–2016	Late April to late September	430–497	(Zhang et al., 2018)
	Hexi Corridor,Gansu	1751–1952	0.965–1.238	101–137	2009	April 10 to September 20	467–545	Zhang et al. (2016)
Winter wheat	Yangling, Shannxi	1524	0.49	203–385	2013–2018	Late October to early June	361–437	This study
	Weishan, Shandong	1127–1285	0.524–0.689	114–145	2005–2008	Mid October to late May	320–412	(Lei and Yang, 2010)
	Luancheng, Hebei	1104–1319	NA	70–197	2008–2011	Mid October to late May	359–478	Shen et al. (2013)

NA, data not available in the references.

interests or personal relationships that could have appeared to influence the work reported in this paper.

Data Availability

The tower-based EC measurements used in this study can be accessed as described by Wang et al. (2019).

Acknowledgments

This work was supported by the National Natural Science Foundation of China, China (51879223 and 42105119), the National Key Research and Development Program of China, China (2016YFC0400201), the Fundamental Research Funds for the Central Universities, China (2452021036), and the 111 Project, China B12007). We thank LetPub (www.letpub.com) for its linguistic assistance during the preparation of this manuscript.

References

Aubinet, M., Vesala, T., Papale, D. (Eds.), 2012. Eddy Covariance: A Practical Guide To Measurement and Data Analysis. Springer Science & Business Media.
Baldocchi, D., 1994. A comparative study of mass and energy exchange over a closed C3 (wheat) and an open C4 (corn) canopy: I. The partitioning of available energy into latent and sensible heat exchange. Agric. Meteorol. 67, 191–220. https://doi.org/10.1016/0168-1923(94)90003-5.
Baldocchi, D., 2008. 'Breathing' of the terrestrial biosphere: lessons learned from a global network of carbon dioxide flux measurement systems. Aust. J. Bot. 56, 1–26. https://doi.org/10.1071/bt07151.
Baldocchi, D., 2014. Measuring fluxes of trace gases and energy between ecosystems and the atmosphere–the state and future of the eddy covariance method. Glob. Change Biol. 20, 3600–3609. https://doi.org/10.1111/gcb.12649.
Baldocchi, D., Falge, E., Gu, L., Olson, R., Hollinger, D., Running, S., Anthoni, P., Bernhofer, C., Davis, K., Evans, R., 2001. FLUXNET: a new tool to study the temporal and spatial variability of ecosystem-scale carbon dioxide, water vapor, and energy flux densities. Bull. Am. Meteorol. Soc. 82, 2415–2434. https://doi.org/10.1175/1520-0477(2001)082<2415:fantts>2.3.co;2.
Baldocchi, D.D., 2003. Assessing the eddy covariance technique for evaluating carbon dioxide exchange rates of ecosystems: past, present and future. Glob. Change Biol. 9, 479–492. https://doi.org/10.1046/j.1365-2486.2003.00629.x.
Baldocchi, D.D., Xu, L., Kiang, N., 2004. How plant functional-type, weather, seasonal drought, and soil physical properties alter water and energy fluxes. Agric. Meteorol. 123, 13–39. https://doi.org/10.1016/j.agrformet.2003.11.006.
Bowen, I.S., 1926. The ratio of heat losses by conduction and evaporation from any water surface. Phys. Rev. 27, 779–787. https://doi.org/10.1103/physrev.27.779.
Burba, G.G., Verma, S.B., 2005. Seasonal and interannual variability in evapotranspiration of native tallgrass prairie and cultivated wheat ecosystems. Agric. Meteorol. 135, 190–201. https://doi.org/10.1016/j.agrformet.2005.11.017.
Businger, J., Wyngaard, J.C., Izumi, Y., Bradley, E.F., 1971. Flux-profile relationships in the atmosphere surface layer. J. Atmos. Sci. 28, 181–189. https://doi.org/10.1175/1520-0469(1971)028<0181:FPRITA>2.0.CO;2.
Byrne, M.P., O'Gorman, P.A., 2013. Land-ocean warming contrast over a wide range of climates: convective quasi-equilibrium theory and idealized simulations. J. Clim. 26 (12), 4000–4016. https://doi.org/10.1175/JCLI-D-12–00262.1.
Damour, G., Simonneau, T., Cochard, H., Urban, L., 2010. An overview of models of stomatal conductance at the leaf level. Plant Cell Environ. 33 (9), 1419–1438. https://doi.org/10.1111/j.1365–3040.2010.02181.x.
Ding, R., Kang, S., Vargas, R., Zhang, Y., Hao, X., 2013. Multiscale spectral analysis of temporal variability in evapotranspiration over irrigated cropland in an arid region. Agric. Water Manag. 130, 79–89. https://doi.org/10.1016/j.agwat.2013.08.019.
Ding, R., Kang, S., Zhang, Y., Hao, X., Tong, L., Li, S., 2015. A dynamic surface conductance to predict crop water use from partial to full canopy cover. Agric. Water Manag. 150, 1–8. https://doi.org/10.1016/j.agwat.2014.11.010.
Edwards, J.R., Lambert, L.S., 2007. Methods for integrating moderation and mediation: a general analytical framework using moderated path analysis. Psychol. Methods 12 (1), 1. https://doi.org/10.1037/1082-989X.12.1.1.
Falge, E., Baldocchi, D., Olson, R., Anthoni, P., Aubinet, M., Bernhofer, C., Burba, G., Ceulemans, R., Clement, R., Dolman, H., 2001. Gap filling strategies for defensible annual sums of net ecosystem exchange. Agric. Meteorol. 107, 43–69. https://doi.org/10.1016/j.agrformet.2006.03.003.
Foken, T., 2008. The energy balance closure problem: an overview. Ecol. Appl. 18, 1351–1367. https://doi.org/10.1890/06-0922.1.
Gao, X., Mei, X., Gu, F., Hao, W., Gong, D., Li, H., 2018. Evapotranspiration partitioning and energy budget in a rainfed spring maize field on the Loess Plateau, China. CATENA 166, 249–259. https://doi.org/10.1016/j.catena.2018.04.008.
Gong, X., Qiu, R., Sun, J., Ge, J., Li, Y., Wang, S., 2020. Evapotranspiration and crop coefficient of tomato grown in a solar greenhouse under full and deficit irrigation. Agric. Water Manag. 235. https://doi.org/10.1016/j.agwat.2020.106154.
Gu, S., Tang, Y., Cui, X., Kato, T., 2005. Energy exchange between the atmosphere and a meadow ecosystem on the Qinghai–Tibetan Plateau. Agric. For. Meteorol. 129, 175–185. https://doi.org/10.1016/j.agrformet.2004.12.002.
Huxman, T.E., Turnipseed, A.A., Sparks, J.P., Harley, P.C., Monson, R.K., 2003. Temperature as a control over ecosystem CO_2 fluxes in a high-elevation, subalpine forest. Oecologia 134, 537–546. https://doi.org/10.1007/s00442-002-1131-1, 2003.
Korner, Christian, 2003. Slow in, rapid out – carbon flux studies and Kyoto targets. Science 300, 1242–1243. https://doi.org/10.1126/science.1084460.
Lei, H., Yang, D., 2010. Interannual and seasonal variability in evapotranspiration and energy partitioning over an irrigated cropland in the North China Plain. Agric. Meteorol. 150, 581–589. https://doi.org/10.1016/j.agrformet.2010.01.022.
Li, L., Yu, Q., 2007. Quantifying the effects of advection on canopy energy budgets and water use efficiency in an irrigated wheat field in the North China Plain. Agric. Water Manag. 89, 116–122. https://doi.org/10.1016/j.agwat.2006.12.003.
Li, S., Zhang, L., Kang, S., Tong, L., Du, T., Hao, X., Zhao, P., 2015. Comparison of several surface resistance models for estimating crop evapotranspiration over the entire growing season in arid regions. Agric. For. Meteorol. 208, 1–15. https://doi.org/10.1016/j.agrformet.2015.04.002.
Li, S., Li, S., Li, Y., Li, X., Tian, X., Zhao, A., Wang, S., Wang, S., Shi, J., 2016. Effect of straw management on carbon sequestration and grain production in maize. Soil Tillage Res. 157, 43–51. https://doi.org/10.1016/j.still.2015.11.002.
Li, S.-G., Eugster, W., Asanuma, J., Kotani, A., Davaa, G., Oyunbaatar, D., Sugita, M., 2006. Energy partitioning and its biophysical controls above a grazing steppe in central Mongolia. Agric. For. Meteorol. 137, 89–106. https://doi.org/10.1016/j.agrformet.2006.03.010.
Li, Z., 2005. Energy balance closure at ChinaFLUX sites. Sci. China 48, 51–62. https://doi.org/10.1360/05zd0005.

Ma, N., Zhang, Y., Guo, Y., Gao, H., Zhang, H., Wang, Y., 2015. Environmental and biophysical controls on the evapotranspiration over the highest alpine steppe. J. Hydrol. 529, 980–992. https://doi.org/10.1016/j.jhydrol.2015.09.013.

Marques, T.V., Mendes, K., Mutti, P., Medeiros, S., Silva, L., Perez-Marin, A.M., Campos, S., Lucio, P.S., Lima, K., Reis, J., Ramos, T.M., Silva, D.F., Oliveira, C.P., Costa, G.B., Antonino, A.C.D., Menezes, R.S.C., Silva, C.M.S., Bezerra, B., 2020. Environmental and biophysical controls of evapotranspiration from Seasonally Dry Tropical Forests (Caatinga) in the Brazilian Semiarid. Agric. Meteorol. 287, 107957 https://doi.org/10.1016/j.agrformet.2020.107957.

Massman, W.J., 1992. A surface energy balance method for partitioning evapotranspiration data into plant and soil components for a surface with partial canopy cover. Water Resour. Res. 28, 1723–1732. https://doi.org/10.1029/92WR00217.

Massmann, A., Gentine, P., Lin, C., 2019. When does vapor pressure deficit drive or reduce evapotranspiration? J. Adv. Model. Earth Syst. 11 (10), 3305–3320. https://doi.org/10.1029/2019MS001790.

McNaughton, K., Spriggs, T., 1986. A mixed-layer model for regional evaporation. Bound. Layer Meteorol. 34, 243–262. https://doi.org/10.1007/bf00122381.

Medlyn, B.E., De Kauwe, M.G., Lin, Y.-S., Knauer, J., Duursma, R.A., Williams, C.A., Arneth, A., Clement, R., Isaac, P., Limousin, J.-M., Linderson, M.-L., Meir, P., Martin-StPaul, N., Wingate, L., 2017. How do leaf and ecosystem measures of water-use efficiency compare? New Phytol. 216 (3), 758–770.

Meyers, T.P., Hollinger, S.E., 2004. An assessment of storage terms in the surface energy balance of maize and soybean. Agric. Meteorol. 125, 105–115. https://doi.org/10.1016/j.agrformet.2004.03.001.

Monteith, J.L., 1965. Symposia of the Society for Experimental Biology, 19, 4.

Paulson, C.A., 1970. The mathematical representation of wind and temperature profiles in the unstable atmosphere surface layer. J. Appl. Meteorol. 9, 857–861. https://doi.org/10.1175/1520-0450(1970)009<0857:TMROWS>2.0.CO;2.

Penman, H.L., 1948. Natural evaporation from open water, bare soil and grass. Proc. R. Soc. Lond. Sect. A 193, 120–145.

Ping, Y., Qiang, Z., Yang, Y., Zhang, L., Zhang, H., Hao, X., Sun, X., 2018. Seasonal and inter-annual variability of the Bowen smith ratio over a semi-arid grassland in the Chinese Loess Plateau. Agric. Meteorol. 252, 99–108. https://doi.org/10.1016/j.agrformet.2018.01.006.

Priestley, C., Taylor, R., 1972. On the assessment of surface heat flux and evaporation using large-scale parameters. Mon. Weather Rev. 100, 81–92. https://doi.org/10.1175/1520-0493(1972)100<0081:otaosh>2.3.co;2.

Prueger, J., Hipps, L., Cooper, D., 1996. Evaporation and the development of the local boundary layer over an irrigated surface in an arid region. Agric. Meteorol. 78, 223–237. https://doi.org/10.1016/0168-1923(95)02234-1.

Rigden, A.J., Salvucci, G.D., 2017. Stomatal response to humidity and CO_2 implicated in recent decline in US evaporation. Glob. Change Biol. 23 (3), 1140–1151.

Rodrigues, T.R., Vourlitis, G.L., de A. Lobo, F., Oliveira, R.G., de S. Nogueira, J., 2014. Seasonal variation in energy balance and canopy conductance for a tropical savanna ecosystem of south central Mato Grosso, Brazil. J. Geophys. Res. Biogeosci. 119, 1–13. https://doi.org/10.1002/2013jg002472.

Ryu, Y., Baldocchi, D.D., Ma, S., Hehn, T., 2008. Interannual variability of evapotranspiration and energy exchange over an annual grassland in California. J. Geophys. Res. 113, D09104. https://doi.org/10.1029/2007JD009263.

Salvucci, G.D., Gentine, P., 2013. Emergent relation between surface vapor conductance and relative humidity profiles yields evaporation rates from weather data. Proc. Natl. Acad. Sci. USA 110 (16), 6287–6291. https://doi.org/10.1073/pnas.1215844110.

Shen, Y., Zhang, Y., Scanlon, B.R., Lei, H., Yang, D., Yang, F., 2013. Energy/water budgets and productivity of the typical croplands irrigated with groundwater and surface water in the North China Plain. Agric. Meteorol. 181, 133–142. https://doi.org/10.1016/j.agrformet.2013.07.013.

Suyker, A.E., Verma, S.B., 2008. Interannual water vapor and energy exchange in an irrigated maize-based agroecosystem. Agric. Meteorol. 148, 417–427. https://doi.org/10.1016/j.agrformet.2007.10.005.

Tan, Z.H., Zhao, J.F., Wang, G.Z., Chen, M.P., Yang, L.Y., He, C.S., Restrepo-Coupe, N., Peng, S.S., Liu, X.Y., da Rocha, H.R., Kosugi, Y., Hirano, T., Saleska, S.R., Foulden, M. L., Zeng, J., Ding, F.J., Gao, F., Song, L., 2019. Surface conductance for evapotranspiration of tropical forests: calculations, variations, and controls. Agric. Meteorol. 275, 317–328. https://doi.org/10.1016/j.agrformet.2019.06.006.

Tang, Y., Wen, X., Sun, X., Wang, H., 2014. Interannual variation of the Bowen ratio in a subtropical coniferous plantation in southeast China, 2003–2012. PLoS One 9 (2), e88267. https://doi.org/10.1371/journal.pone.0088267.

Tian, F., Yang, P., Hu, H., Liu, H., 2016. Energy balance and canopy conductance for a cotton field under film mulched drip irrigation in an arid region of northwestern China. Agric. Water Manag. 179. https://doi.org/10.1016/j.agwat.2016.06.029.

Tong, X.-J., Li, J., Yu, Q., Qin, Z., 2009. Ecosystem water use efficiency in an irrigated cropland in the North China Plain. J. Hydrol. 374, 329–337. https://doi.org/10.1016/j.jhydrol.2009.06.030.

Twine, T.E., Kustas, W.P., Norman, J.M., Cook, D.R., Houser, P.R., Meyers, T.P., Prueger, J.H., Starks, P.J., Wesely, M.L., 2000. Correcting eddy-covariance flux underestimates over a grassland. Agric. Meteorol. 103 (3), 0–300.

Wang, Y., Cai, H.J., Yu, L.Y., Peng, X.B., Xu, J.T., Wang, X.W., 2020a. Evapotranspiration partitioning and crop coefficient of maize in dry semi-humid climate regime. Agric. Water Manag. 236, 106164 https://doi.org/10.1016/j.agwat.2020.106164.

Wang, Y., Zeng, Y., Yu, L., Yang, P., Van de Tol, C., Cai, H., Su, Z., 2020b. Integrated modeling of canopy photosynthesis, fluorescence, and the transfer of energy, mass, and momentum in the soil–plant–atmosphere continuum (STEMMUS–SCOPE v1. 0.0). Geosci. Model Dev. 14 (3), 1379–1407. https://doi.org/10.5194/gmd-14-1379-2021.

Wang, Y., Cai, H.J., Zeng, Y.J., Su, Z., Yu, L.Y., 2019. Data underlying the research on Seasonal and interannual variation in evapotranspiration, energy flux, and Bowen ratio over a dry semi-humid cropland in Northwest China, 4TU. Centre for Research Data. Dataset. https://doi.org/10.4121/uuid:aa0ed483-701e-4ba0-b7b0-674695f5f7a7.

Webb, E.K., Pearman, G.I., Leuning, R., 1980. Correction of flux measurements for density effects due to heat and water vapour transfer. Q. J. R. Meteorol. Soc. 106, 85–100. https://doi.org/10.1256/smsqj.44706.

Widmoser, P., Wohlfahrt, G., 2018. Attributing the energy imbalance by concurrent lysimeter and eddy covariance evapotranspiration measurements. Agric. Meteorol. 263, 287–291. https://doi.org/10.1016/j.agrformet.2018.09.003.

Wilczak, J.M., Oncley, S.P., Stage, S.A., 2001. Sonic anemometer tilt correction algorithms. Bound. -Layer Meteorol. 99, 127–150. https://doi.org/10.1023/a:1018966204465.

Wilson, K., Goldstein, A., Falge, E., Aubinet, M., Baldocchi, D., Berbigier, P., Bernhofer, C., Ceulemans, R., Dolman, H., Field, C., 2002. Energy balance closure at FLUXNET sites. Agric. Meteorol. 113, 223–243. https://doi.org/10.1016/s0168-1923(02)00109-0.

Wilson, K.B., Baldocchi, D.D., 2000. Seasonal and interannual variability of energy fluxes over a broadleaved temperate deciduous forest in North America. Agric. Meteorol. 100, 1–18. https://doi.org/10.1016/s0168-1923(99)00088-x.

Wofsy, S., Goulden, M., Munger, J., Fan, S.M., Bakwin, P., Daube, B., Bassow, S., Bazzaz, F., 1993. Net exchange of CO_2 in a mid-latitude forest. Science 260, 1314–1317. https://doi.org/10.1126/science.260.5112.1314.

Wu, J., Guan, D., Han, S., Shi, T., Jin, C., Pei, T., Yu, G., 2007. Energy budget above a temperate mixed forest in northeastern China. Hydrol. Process.: Int. J. 21, 2425–2434. https://doi.org/10.1002/hyp.6395.

Xu, S., Yu, Z., Zhang, K., Ji, X., Yang, C., Sudicky, E.A., 2018. Simulating canopy conductance of the *Haloxylon ammodendron* shrubland in an arid inland river basin of northwest China. Agric. Meteorol. 249, 22–34. https://doi.org/10.1016/j.agrformet.2017.11.015.

Yang, D., Sun, F., Liu, Z., Cong, A., Ni, G., Lei, Z., 2007. Analyzing spatial and temporal variability of annual water-energy balance in nonhumid regions of China using the Budyko hypothesis. Water Resour. Res. 43, 4. https://doi.org/10.1029/2006wr005224.

Yu, L., Zeng, Y., Su, Z., Cai, H., Zheng, Z., 2016. The effect of different evapotranspiration methods on portraying soil water dynamics and ET partitioning in a semi-arid environment in Northwest China. Hydrol. Earth Syst. Sci. 20, 975–990. https://doi.org/10.5194/hess-20-975-2016.

Yu, L., Zeng, Y., Wen, J., Su, Z., 2018. Liquid-vapor-air flow in the frozen soil. J. Geophys. Res. -Atmos. 123, 7393–7415. https://doi.org/10.1029/2018JD028502.

Zha, T., Li, C., Kellomäki, S., Peltola, H., Wang, K.Y., Zhang, Y., 2013. Controls of evapotranspiration and CO_2 fluxes from scots pine by surface conductance and abiotic factors. PLoS One 8. https://doi.org/10.1371/journal.pone.0069027.

Zhang, Y., Wang, J., Gong, S., Xu, D., Sui, J., Wu, Z., Mo, Y., 2018. Effects of film mulching on evapotranspiration, yield and water use efficiency of a maize field with drip irrigation in Northeastern China. Agric. Water Manag. 205, 90–99. https://doi.org/10.1016/j.agrformet.2016.04.002.

Zhang, Y., Zhao, W., He, J., Zhang, K., 2016. Energy exchange and evapotranspiration over irrigated seed maize agroecosystems in a desert-oasis region, northwest China. Agric. Meteorol. 223, 48–59. https://doi.org/10.1016/j.agrformet.2016.04.002.

Zhao, H., Shar, A.G., Li, S., Chen, Y., Shi, J., Zhang, X., Tian, X., 2018. Effect of straw return mode on soil aggregation and aggregate carbon content in an annual maize-wheat double cropping system. Soil Tillage Res. 175, 178–186. https://doi.org/10.1016/j.still.2017.09.012.

Zheng, J., Wang, H., Fan, J., Zhang, F., Guo, J., Liao, Z., Zhuang, Q., 2021. Wheat straw mulching with nitrification inhibitor application improves grain yield and economic benefit while mitigating gaseous emissions from a dryland maize field in northwest China. Field Crops Res. 265 (108125) https://doi.org/10.1016/j.fcr.2021.108125.

Zhuang, W., Cheng, L., Whitley, R., Shi, H., Beringer, J., Wang, Y., He, L., Cleverly, J., Eamus, D., Yu, Q., 2016. How energy and water availability constrain vegetation water-use along the North Australian Tropical Transect. Int. J. Plant Prod. 10, 403–423.